Flexible Visible–Infrared Metamaterials and Their Applications in Highly Sensitive Chemical and Biological Sensing

ARTICLE *in* NANO LETTERS · JUNE 2011

Impact Factor: 13.59 · DOI: 10.1021/nl2014982 · Source: PubMed

8 AUTHORS, INCLUDING:

Bo Peng
Nanyang Technological University
227 PUBLICATIONS **4,198** CITATIONS
SEE PROFILE

Dehui Li
Nanyang Technological University
39 PUBLICATIONS **721** CITATIONS
SEE PROFILE

Jun Zhang
Chinese Academy of Sciences
54 PUBLICATIONS **1,013** CITATIONS
SEE PROFILE

Qihua Xiong
Nanyang Technological University
166 PUBLICATIONS **3,984** CITATIONS
SEE PROFILE

NANO LETTERS

LETTER

pubs.acs.org/NanoLett

Flexible Visible−Infrared Metamaterials and Their Applications in Highly Sensitive Chemical and Biological Sensing

Xinlong Xu,[†] Bo Peng,[†] Dehui Li,[†] Jun Zhang,[†] Lai Mun Wong,[‡] Qing Zhang,[†] Shijie Wang,[‡] and Qihua Xiong*[,†,§]

[†]Division of Physics and Applied Physics, School of Physical and Mathematical Sciences, Nanyang Technological University, Singapore 637371

[‡]Institute of Materials Research & Engineering, Agency for Science, Technologies and Research, 3 Research Link, Singapore 117602

[§]Division of Microelectronics, School of Electrical and Electronic Engineering, Nanyang Technological University, Singapore 639798

ABSTRACT: Flexible electronic and photonic devices have been demonstrated in the past decade, with significant promise in low-cost, light-weighted, transparent, biocompatible, and portable devices for a wide range of applications. Herein, we demonstrate a flexible metamaterial (Metaflex)-based photonic device operating in the visible−IR regime, which shows potential applications in high sensitivity strain, biological and chemical sensing. The metamaterial structure, consisting of split ring resonators (SRRs) of 30 nm thick Au or Ag, has been fabricated on poly(ethylene naphthalate) substrates with the least line width of ∼30 nm by electron beam lithography. The absorption resonances can be tuned from middle IR to visible range. The Ag U-shaped SRRs metamaterials exhibit an electric resonance of ∼542 nm and a magnetic resonance of ∼756 nm. Both the electric and magnetic resonance modes show highly sensitive responses to out-of-plane bending strain, surrounding dielectric media, and surface chemical environment. Due to the electric and magnetic field coupling, the magnetic response gives a sensitivity as high as 436 nm/RIU. Our Metaflex devices show superior responses with a shift of magnetic resonance of 4.5 nm/nM for nonspecific bovine serum albumin protein binding and 65 nm for a self-assembled monolayer of 2-naphthalenethiol, respectively, suggesting considerable promise in flexible and transparent photonic devices for chemical and biological sensing.

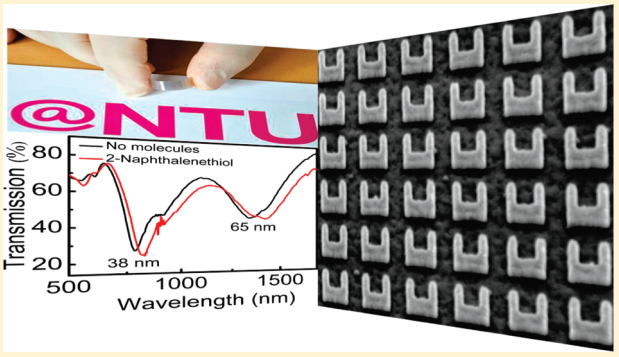

KEYWORDS: Flexible metamaterials, split-ring resonators, strain sensor, chemical sensor, biosensor

Integration of functional high-performance electronic devices onto mechanically flexible and deformable substrates offers significant promise in flexible electronics such as flexible displays,[1,2] solar cells,[3] nanowire electronics,[4] and sensing circuitry.[5−7] Compared to rigid substrates such as silicon and glass, flexible and stretchable plastic or elastomer based substrates exhibit great advantages of flexibility, transparency, lightweight, portability, low cost, conformable manipulation, and biocompatibility. On the other hand, the recent development of transformation optics offers an alternative arithmetic based on the topological design and manipulation of light,[8,9] which makes flexible functional optics a promising way to control optical waves, thus leading to the integration of functional flexible photonic devices as recently demonstrated in strained tunability applications.[10]

Recently, metamaterials have been shown as an effective way to enhance the manipulation of optics. By properly designing the "artificial atoms" such as split ring resonators (SRRs) within a metamaterial, one can create materials with optical properties beyond the limitations of conventional, naturally occurring material or composites. This has been demonstrated in microwave,[11] infrared,[12] and terahertz regions.[13] Realization of electromagnetic response for metamaterials in the visible and infrared (vis−IR) regions may open a whole new era of photonics connected with novel concepts and potential applications,[14,15] such as security imaging, remote sensing, and switchable and transformable optical frequency resonant devices.[16] Nevertheless it is still quite challenging to push the metamaterial to operate in the visible optical frequency, as it requires fabricating the structures down to the tens of nanometers regime.

Attributing flexibility to metamaterials also has profound interest. For example, such flexibility makes it possible to "wrap" light-weight, transparent metamaterials around important objects as an optical cloak. The flexible metamaterials (Metaflex) have been demonstrated mainly in microwave and terahertz regions,[17,18] but with a limited access to the optical region as discussed recently by Falco et al., who believed that electron beam lithography (EBL) requires a rigid and flat substrate.[19] Thus an indirect transfer method was usually used to embed metamaterials into a flexible elastomeric matrix after the metamaterials

Received: May 5, 2011
Revised: June 12, 2011
Published: June 22, 2011

were fabricated onto rigid and flat substrates such as silicon and quartz.[10]

We demonstrate in this paper that commercial flexible plastic substrate is actually compatible for critical EBL nanofabrication with the least feature size down to 30 nm. We tune the SRR-based metamaterials size directly with the least line width from 80 to 30 nm. Correspondingly, the electric response resonances shift from 975 nm (1088 nm) to 542 nm (653 nm), while the magnetic response resonances shift from 1687 nm (>1700 nm) to 756 nm (902 nm) for Ag (Au) metamaterials, respectively. Due to a strong coupling in optical frequency, the electric resonance shows an exponential dependence on the feature size. The finite difference time-domain (FDTD) method is used to simulate the electromagnetic response of the metamaterials, which shows a good agreement with the measurements. We further demonstrate that this vis−IR Metaflex exhibits a very sensitive response to the strain, the dielectric media, and the surface chemical and biological local environment, suggesting that flexible metamaterials exhibit significant promise as excellent photonic devices for highly sensitive strain, chemical and biological sensing applications.

SRRs was first introduced by Pendry et al.[20] as an important optical component for metamaterials which may exhibit both electric and magnetic resonance,[12−14,21] of which the latter being commonly absent in other components such as metallic wires and meshes. Experiments have revealed the fascinating electromagnetic properties of SRR combination with wires, such as negative refractive index[22] and three-dimensional coupling of SRRs.[23] It requires much more technological effort to push the SRR resonances operating in the visible region than in the microwave and terahertz regions. The geometrical parameters that describe the U-shape SRRs demonstrated in this paper are shown in Figure 1a. The periodicities of the unit cell along x axis and y axis are 504 and 480 nm, respectively. In order to push the electric response from the infrared to visible region, the whole unit size of SRRs including the unit cell is reduced to 37.5% (100% corresponds to original size defined in Figure 1a), which decreases the w from 80 to 30 nm. The pattern was fabricated using EBL on poly(ethylene naphthalate) (PEN) substrates (Teijin DuPont Films). The PEN substrates were first sputtered a layer of ITO with a thickness of 100 nm to decrease the charging effect. Commercial electron beam resist PMMA (950 A4, Microchem, USA) was spin-coated at 4000 rpm and baked at 180 °C. A JEOL 7001F SEM equipped with a nanometer pattern generation system (NPGS) was used to define the patterns. After development, a metal film of Ag or Au (∼30 nm) with a 2 nm Cr film as an adhesion layer was deposited using thermal evaporation (Elite Engineering, Singapore). Figure 1b summarizes the SEM (JEOL 7001F) images of the unit cells of the Ag SRRs for w = 80−30 nm (from left to right, all the scale bars are 100 nm). Figure 1c shows a typical SEM image of SRRs on PEN with a designed w = 80 nm, where the actual width exhibits ±7% standard deviation after statistical analysis. It is important to note that the focus and beam alignment are very critical to achieve good pattern fidelity.

The transmission spectra were taken on a microspectrophotometer (Craic 2000) in the range of 300−1700 nm. To predict the spectra thus guide us in pattern design even before fabrication and measurement, FDTD calculations based on MEEP codes were performed,[24] with the dielectric constant of Ag based on a Drude model obtained from Blaber et al.[25] The dielectric constant of Au for calculation was obtained from ref 14. Figure 2a

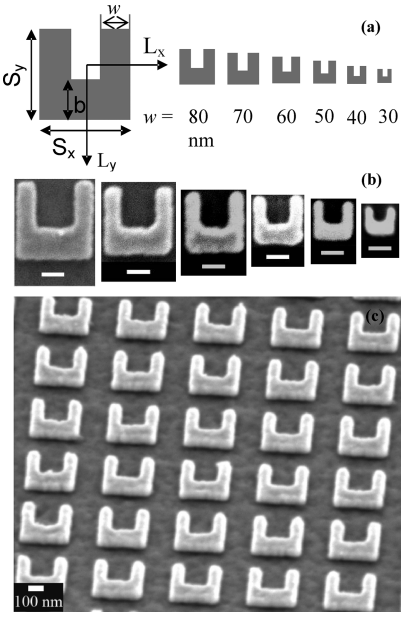

Figure 1. (a) A schematic diagram of SRRs with L_x = 504 nm, L_y = 480 nm, S_x = S_y = 320 nm, w = 80 nm, and b = 128 nm. The whole unit size and the periodicity of the unit cell were decreased accordingly in order to push to visible regime. The actual width w is specified in the right. (b) SEM images of the unit cells of the SRRs for w = 80−30 nm (from left to right, scale bars 100 nm). (c) A typical SEM image (45° tilted) of SRRs with w = 80 nm fabricated on a PEN substrate.

displays transmission spectra as a dependence on w of SRRs for Ag SRRs. Two main absorption peaks were identified. The one with the shorter wavelength tuned to the visible region corresponds to the electric resonance. With the increase of size, the electric response exhibits a systematic red shift. The other resonance in the longer wavelength has been tuned from the mid-infrared (1687 nm) to visible region (756 nm), which corresponds to the magnetic response and it also shows red shift as the size of SRR increases. The magnetic response is due to the molecular loop current when the electric polarization is along the gap-bearing side of SRRs.[12,14,21] We used an unpolarized light source, and thus the calculations were performed by averaging the polarization effect for both transverse magnetic (TM) and transverse electric (TE). Usually, few natural materials exhibit magnetic response above the microwave region.[12,13] Since the development of metamaterials, there has been an extensive effort to push the magnetic response to a higher frequency regime. For instance, Yen et al.[13] first demonstrated the magnetic response with double ring SRRs in the terahertz region and then Linden et al. pushed the magnetic response to 100 THz with a single ring SRR.[12] Enkrich et al. further pushed the magnetic mode to the telecommunication region and demonstrated a record of 200 THz for the fundamental magnetic mode and 370 THz for high order magnetic resonance for oblique incidence.[14] Hence, the fundamental magnetic response at 756 nm (396.6 THz) of our metamaterials represents the highest frequency so far in the visible region with SRR-based metamaterials. The weak peaks before the electric resonances in Figure 2a on the shorter wavelength side could be the higher order multipolar modes as suggested by Rockstuhl et al.[26]

In Figure 2b we also show the simulation results for different w values that we fabricated, suggesting a good agreement with our

dx.doi.org/10.1021/nl2014982 |Nano Lett. 2011, 11, 3232–3238

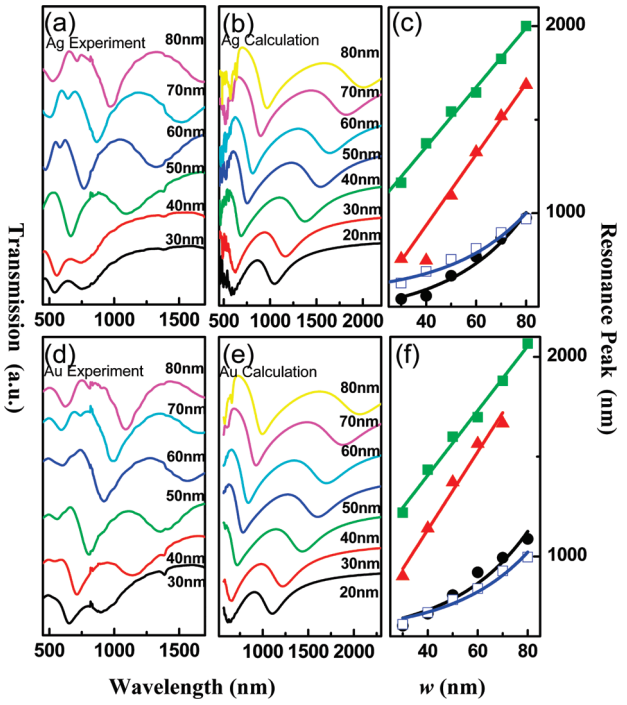

Figure 2. (a) Experimental transmission spectra of SRRs with different side widths of w as shown in Figure 1 for Ag metamaterials. (b) Calculated transmission spectra of SRRs by FDTD for Ag metamaterials. (c) Experimental magnetic (red triangles), electric resonance peaks (black circles), calculated magnetic (green squares), and electric resonant peak (blue squares) as a function of w for Ag metamatierlas. The curves in (c) are fitting curves as discussed in the text. (d) Experimental transmission spectra of SRRs with different side widths of w for Au metamaterials. (e) Calculated transmission spectra of SRRs for Au metamaterials. (f) Experimental magnetic (red triangles), electric resonance peaks (black circles), calculated magnetic (green squares), and electric resonance peak (blue squares) as a function of w for Au metamaterials. The curves in (f) are fitting lines as discussed in the text.

experimental spectra. The slight difference is attributed to the size distribution of the pattern resulting from fabrication. Panels d and e of Figure 2 display the results of the experimental and calculated transmission spectra for Au-based SRRs. The electric response resonances shift from 1088 to 653 nm, while the magnetic response resonances shift from >1700 nm (which is out of our measurement region) to 902 nm. The peak positions of the experimental spectra and simulations are extracted and plotted in panels c and f of Figure 2 as a function of wavelength for various w values for Ag and Au, respectively. In Figure 2c, the circle points (black) are the experimental values of electric resonance and the solid curves are the fitting lines with an empirical formula of $\lambda = \lambda_0 + a \exp(w/w_1)$. Where λ is the resonance position, $w_1 = 30$ nm is the least width of our patterns, and $\lambda_0 = 446 \pm 27$ nm is the convergence of the fitting. $a = 39 \pm 4$ is the growth ratio demonstrating the scaling behavior. λ_0 approaches the resonant wavelength of localized plasmon resonance (LPR) of silver nanoparticles in the range of 400−600 nm and is the limit of electric response when the size is further decreased. The calculated size dependence of the resonance position shows a similar dependence with the experiments with the squared points (blue). Using the same formula for fitting, we get $\lambda_0 = 562 \pm 21$ nm and $a = 31 \pm 3$. This empirical formula captures the main physics embodied in our observations. Two factors affect the scaling behavior of our SRRs metamaterials. One is the resonance wavelength which is red-shifted with the unit cells. From the LC resonance point of view, the resonance frequency can be expressed as a combination of capacitance and inductance with the formula $\omega_{LC} = (LC)^{-1/2}$.[12,27,28] With the increase of the unit cell size, the capacitance and inductance increase and the resonance frequency decreases accordingly. The other is the coupling between unit cells due to the decreasing of periodicity. For the metallic particle−particle interaction, the coupling between the unit cells results in an exponential decay of resonances and blue shifts with the increasing of particle−particle distance.[29,30] The red shift as unit size and periodicity increase in Figure 2a suggests that the main contribution comes from the first factor.

Recently, Falco et al.[19] demonstrated a Metaflex with the electric resonance near 620 nm with a fishnet geometry, which is less challenging to fabricate in the visible region with low quality factor of resonance. We show here that an electric resonance near 542 nm for Ag with SRR-based metamaterials can be achieved by directly patterning on plastic substrates by EBL fabrication. To our best knowledge, this is the first time such a short wavelength in the visible region can be achieved for the SRR-based metamaterials. The experimental data of electric resonance peaks in Figure 2f show the similar dependence on the unit size for Au metamaterials as for Ag metamaterials. The fitting for experimental data yields $\lambda_0 = 591 \pm 36$ nm and $a = 37 \pm 4$.

The resonance peak of the magnetic response for Ag metamaterials shows a linear dependence on size with an intercept of approximately 177 ± 34 nm and a slope of 19 ± 1 nm as shown in Figure 2c. The experimental point falls outside the fitting line for magnetic resonance at 40 nm probably due to deviation of size, especially the arms of SRRs, which will influence the formation of the loop current. The coupling between the artificial magnetic dipoles is weaker compared with the electric dipoles, which shows exponential dependence on resonance wavelength. From dipole−dipole interaction point of view, the quasi-static interaction energy ΔE is written as[27]

$$\Delta E = \gamma \frac{p_1 p_2}{4\pi\varepsilon_0 r^3} \quad (1)$$

where r is the distance between dipoles p_1 and p_2. γ is the interaction index, which is 1 for transverse coupling (in our case for the magnetic resonance) and 2 for longitudinal coupling (in our lateral coupling for electrical resonance). Considering the electrical dipoles are stronger than the magnetic dipoles (with sharper electric resonance compared with magnetic resonance), the coupling of electric dipoles is stronger than that of magnetic dipoles. Figure 2c also displays the unit size dependence of the calculated resonance position with an intercept of 717 ± 26 nm and a slope of 16 ± 1 nm. The combination of red shift due to the unit size increase and the coupling between SRRs results in the linear dependence of the magnetic resonance peak on the unit cell size. Similar results have been shown for Au metamaterials as in Figure 2f with the linear fitting.

PEN was chosen as the plastic substrate because it has a high glass transition temperature ($T_g \approx 125$ °C) than some other polymers such as poly(ethylene terephthalate) (PET $T_g \approx 80$ °C). PEN is also solvent, acid, and base resistant. Flexible PEN substrate has a Young's modulus (E) of 280 MPa (characteristics of physical properties by Teijin DuPont Films Co.) and the PEN substrates used here have thickness (t) of ~125 μm. The transparency in the visible and near-infrared region is over

dx.doi.org/10.1021/nl2014982 |Nano Lett. 2011, 11, 3232–3238

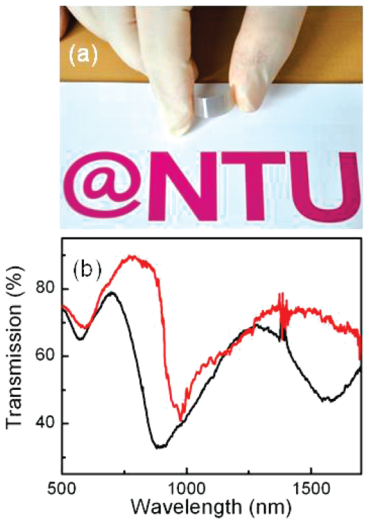

Figure 3. (a) A picture of our Metaflex taken with a background of NTU campus magazine to demonstrate the flexibility. (b) Transmission spectra of Metaflex showing high tunability with an out-of-plane strain. Black and red curves are the transmission spectra before and after applying the strain, respectively.

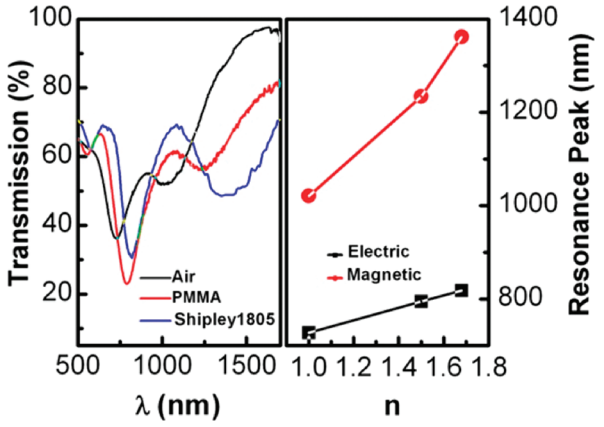

Figure 4. (a) Transmission spectra of Metaflex (Au film with $w = 40$ nm) taken in air (black), with a layer of PMMA (red) and with a layer of Shipley 1805 (blue). (b) Resonance peak positions as a function of refractive index.

80%, which is adequate for transparent photonic devices. In addition, the mechanical characteristics of PEN make it ideal to test how optical properties of metamaterials respond to the strain of the out-of-plane direction.

Figure 3 demonstrates the strain sensing by PEN-based metamaterials of Au with $w = 50$ nm with a deflection ratio of 1%. From the stress $\delta = t/\rho = 4.4 \times 10^{-6}$ (ρ is the radius of the arc after bending), the strain $\sigma = E\delta$ is approximately 1232 Pa. The electric peak position shifts from 894 to 973 nm, giving a net shift of 79 nm, while the magnetic response has moved out of our measurable region. The strain sensitivity was estimated to be ~0.06 nm/Pa. Tunability of metamaterials by stretching in the infrared region has been demonstrated by Pryce et al.,[10] using pattern transfer of SRRs from silicon substrate to PDMS media after EBL fabrication. Here we demonstrate a direct EBL fabrication of metamaterials on plastic substrate PEN, which can also be used to integrate into a photonic device compatible with modern optical techniques such as a remote strain sensor to monitor vibrations for some precision instruments.[31]

There are two classes of plasmon based sensing methods reported in the literature. One is based on the surface plasmon polariton (SPP), which has been successfully applied to biochemistry and medical research.[32,33] Another type is based on the LPR from the colloidal nanoparticles.[34] It has been shown that the refractive index sensitivity does not exceed 100−300 nm per RIU in visible spectral interrogation, where RIU represents refractive index unit.[35] Recently, Kabashin et al.[36] utilized the combination of LPR and SPP in the plasmonic nanorod array and demonstrated an enhanced sensitivity to the refractive-index variations of the medium between nanorods. Gu et al. also proved that an X-shape nanohole can increase the sensitivity due to the electric field enhancement created by LPR.[37] Plasmonic nanoholes or nanorods have been used as an excellent sensing platform for a variety of applications such as live viruses[38] and glucose solution.[39,40]

According to the effective medium theory, the resonance frequency of metamaterials is very sensitive to the surrounding refractive index.[36] For instance, dielectric overcoating or multilayer dielectric sandwiching methods have been used to tune the absorption resonance position of metamaterials in the terahertz regime.[28] To investigate how metamaterials in optical frequency regime respond to the change of local dielectric environment, we spin-coated a layer of PMMA onto the metamaterials surface with a thickness of approximately 200 nm. The refractive index of PMMA in the visible and infrared regions is 1.488.[41] PMMA on metamaterials will act as a good model to evaluate how the resonances of metamaterials vary as the dielectric environment changes, providing a direct measurement of the figure of merit of the sensitivity. We also used another photoresist (Shipley 1805) with a refractive index of ~1.68 in the visible and infrared regions. Figure 4a displays the experimental transmission spectra taken in air (black line), with a thin layer of PMMA (red line) and a thin layer of Shipley 1805 (blue line) for the Metaflex with a $w =$ 40 nm. Since Au is more inert than Ag with well established surface functionality, we will focus on Au-based metamaterials for the following sensing applications. The shift for the electric resonance is approximately 67 nm upon PMMA coating and that of the magnetic resonance is approximately 213 nm. The Shipley 1805 also shows similar results with an 90 nm shift in electric mode resonance while a 341 nm shift in magnetic resonance mode, respectively. The sensitivity is estimated to be 137 nm/RIU and 436 nm/RIU for the electric and magnetic responses, respectively. The resonance peak position change with local environmental refractive index change is shown in Figure 4b. The sensitivity of the electric response is comparable to that of the gold nanoparticles based localized surface plasmon biosensing,[35] while the sensitivity evaluated based on magnetic resonance increases by more than twice compared with the electric response.

As a bianisotropic component,[21,42] SRRs show not only the electric response due to the collective oscillations of free electrons in metallic nanostructures, but also the artificial magnetic response due to the electrical field induced molecular loop current at normal incidence. The constitutive relationship between electric component ($\mathbf{E}$), magnetic component ($\mathbf{H}$), electric displacement ($\mathbf{D}$), and magnetic field ($\mathbf{B}$) can be written as,[21]

$$\mathbf{D} = \varepsilon_0\varepsilon_r\mathbf{E} + \xi\mathbf{H}/c, \quad \mathbf{B} = \mu_0\mu_r\mathbf{H} + \chi\mathbf{E}/\mathbf{c} \qquad (2)$$

where ε_r is the relative permittivity and μ_r is the relative permeability, while χ and ξ are the coupling coefficients of magnetic and electric fields in the SRRs, respectively. For electric

dx.doi.org/10.1021/nl2014982 |Nano Lett. 2011, 11, 3232–3238

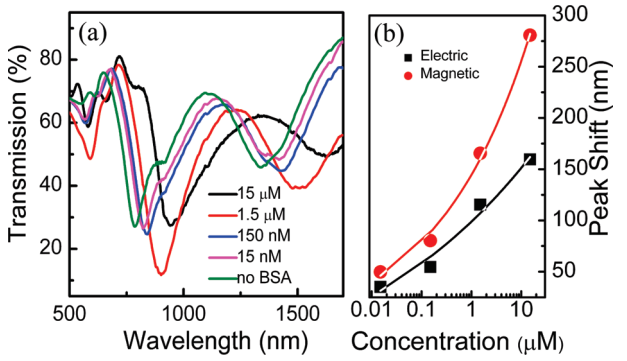

Figure 5. (a) Transmission spectra of the same Metaflex sample after different BSA concentration treatment, ranging from 15 μM to 15 nM. The spectrum of the sample without BSA was provided as a reference. (b) Resonance peak shift as a function of concentration with SRRs. The solid curves are empirical fittings as discussed in the text.

response, the sensing mechanism stems purely from the response of ε_r change from the microenvironments. This mechanism has been applied for both SPP and LPR and also for the electric resonance in SRRs.[35,43] On the other hand, the magnetic response in SRRs originates from the χ, which is due to the electrical and magnetic field coupling. χ can be modeled by a magnetic coil with an inductance L (metal ring) coupled with a capacitance C (the slit of the ring) and the resonance frequency $\omega_{LC} = (LC)^{-1/2}$.[12,27,28] Shelton et al.[44] suggested that the capacitance consisted of two contributions: one is the gap capacitance (C_g) of the SRRs, while the other is fringing-field capacitance (C_f), which depends on the permittivity $C_f \propto \varepsilon_0 \int \varepsilon(\nu) E(\nu)\, d\nu$ and the thickness of the thin film that exists between SRRs and the PEN substrate. The electric resonance is primarily determined by C_f, which is highly dependent on the dielectric environment, while the magnetic resonance is related not only to the C_f but also to the C_g. Therefore, magnetic resonance exhibits higher sensitivity to the surrounding environment.

The high sensitivity of the Metaflex resonance in response to a local effective refractive index change suggests potential applications in chemical and biological sensing. An important category of biomolecules in biosensing is protein, which includes a variety of biomarkers that are extremely important for disease diagnosis and analysis.[45,46] To evaluate whether and how our Metaflex in optical frequency regime detect protein molecules, we used a well-known model protein of bovine serum albumin (BSA) with a molecular weight of 66776 Da. The BSA powder was first dissolved in distilled water with a concentration of 15 μM, and then the solution was diluted to change the concentration from the original 15 μM to 15 nM. The BSA solution was drop-casted on the Metaflex surface, which was then dried under room temperature. Hence, the protein molecules were nonspecifically bound to the metamaterials surface. Transmission spectra were taken afterward under the microspectrophotometer. After the measurement, the *same* chip was soaked in the distilled water and then carefully cleaned with a heavy rinse of distilled water plus an O_2 plasma treatment at 50 W for 30 s. This cleaning method was proven to be effective by retaking the transmission spectra, which gave identical spectra obtained from the same sample before applying BSA. Then a different concentration sample was prepared and measured.

Figure 5a displays a series of spectra of the *same* Metaflex sample with different BSA concentrations. Both the magnetic

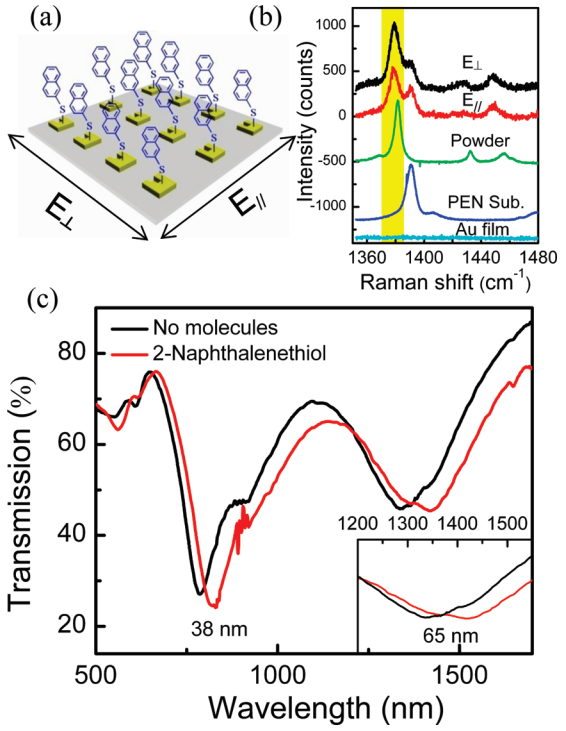

Figure 6. (a) A schematic diagram of chemical sensing of 2-naphthalenethiol using Metaflex. For simplicity, only one 2-naphthalenethiol molecule was drawn on each SRR. (b) Raman spectra of 2-naphthalenethiol on a Metaflex sample with polarization perpendicular or parallel as shown in (a), from 2-naphthalenethiol powder, from a clean PEN substrate, and from a Au film on the same PEN substrate (from top to bottom, spectra were shifted upward for clarity), respectively. (c) Transmission spectra of SRRs with and without 2-naphthalenethiol, the inset is the zoom-in view of the spectra around the magnetic resonance mode. Both peak shifts due to molecule binding are labeled.

and electric response modes are significantly red-shifted. The concentration dependence of the peak position is extracted and plotted in Figure 5b, with red dots representing magnetic resonance and black squares for electric resonance. The solid curves are the least-squares fitting with a formula $\lambda_{shift} = a + b[M]^c$, where [M] is the concentration. The sensitivity can be approximately written as $d\lambda_{shift}/d[M] = bc[M]^{c-1}$, for 15 nM, this can reach 1.8 nm/nM for electric response and 4.5 nm/nM for magnetic response. It is important to note that the sensitivity can be further increased by metamaterial design.[47] For example, a trapped resonance mode was recently demonstrated to exhibit a high quality factor when the structural symmetry was broken, thus higher sensitivity resulted.[48]

The interaction between BSA and Au metamaterials surface is still nonspecific. Specific chemical interaction is needed to further extend the applications of metamaterials to chemical and biological sensing. The metamaterial Au surface can be functionalized via covalent thiol chemistry, and therefore labeling can be readily achieved using thiol-terminated functional groups, e.g., thiolated biotin.[49] Here we further demonstrate a chemical sensing of a monolayer of thiol-terminated molecules that are covalently bound to Au metamaterials surface. Metamaterials-based surface chemical sensing offers a very promising field for sensing applications, which provides a complementary detection besides well-accepted surface-enhanced Raman scattering (SERS) and SPP. The high tunability in the whole range of vis−IR

dx.doi.org/10.1021/nl2014982 |*Nano Lett.* 2011, 11, 3232–3238

spectra regime offers unique advantages to tune the interaction between analyte molecules and surface plasmon, which is not possible in thin film SPP biosensing. As a preliminary demonstration, 2-naphthalenethiol (Sigma-Aldrich, USA) was chosen as a model molecule as schematically shown in Figure 6a.[50] To prepare the sample, 2-naphalenethiol powder was dissolved in ethanol with a concentration of 10 mM. The PEN-based Au metamaterial was soaked in the solution for 24 h and then was heavily rinsed with ethanol followed by drying with nitrogen gas.

To evaluate whether the molecule is indeed chemically bound to metamaterials, Raman scattering spectroscopy was conducted on the Metaflex surface using a micro-Raman spectrometer (Horiba-JY T64,000) excited with a solid state laser (λ = 785 nm) in the backscattering configuration. The backscattered signal was collected through a 50× objective and dispersed by a 1800 g/mm grating, and the laser power on the sample surface was measured to be about 2.5 mW. Figure 6b shows the Raman spectra of 2-naphthalenethiol on metamaterial with two polarization configurations as shown in Figure 6a, from the powder, from clean PEN substrate without metamaterials and from Au film on the same chip from top to bottom, respectively. The Raman peak around 1379.4 cm^{-1} due to ring−ring stretching has been chosen as a comparison.[51] The control spectrum from 2-naphthalenethiol powder shows a ring−ring stretching mode at ∼1381.5 cm^{-1}, which suggests a ∼2 cm^{-1} red shift on the metamaterial surface probably due to charge transfer between gold and the molecule. Usually, chemical absorption by the thiol molecules will modify the Raman polarizability tensor and hence shift the vibrational mode frequency and change Raman intensity as well.[52] The Raman band ∼1390.9 cm^{-1} from PEN as shown in the control spectrum is due to naphthalene ring vibrational mode in PEN.[53] It is important to note that no Raman signal from 2-naphthalenethiol was detected from a Au thin film on the same chip; hence both the thickness and reaction conditions are the same as Metaflex, while the Raman signal from 2-naphalenethiol molecules linked to Metaflex is exceptionally strong. This enhancement is a typical electromagnetic enhancement in the SERS effect.[54]

After that, the transmission spectra of metamaterial structures after 2-naphthalenethiol functionalization have been taken. Compared with spectra taken from bare metamaterials on PEN, the absorption resonance peak exhibits a red shift of about 38 nm for electric resonance mode and about 65 nm for magnetic mode as shown clearly in Figure 6c and inset, respectively. Unlike the data shown in Figures 4 and 5, which are due to the local change of dielectric constant due to binding/coating of PMMA or BSA, the significant peak shift in Figure 6 stems from only the surface chemical modification due to a single layer of 2-naphthalenethiol, which is only on the order of 1 nm thick. Such a significant change of resonance peak of metamaterials due to a single layer chemical molecule binding has not been well studied in the metamaterials community. Recently, a resonance peak shift of ∼160 nm due to a monolayer graphene has been observed for metamaterials generated by a focused ion beam (FIB) at the IR regime.[55] We believe our chemical sensing measurements demonstrate the possibility of sensitive detection and correlation between the peak shift and the length of molecules that bind to the surface. Complemented with a strong SERS effect, our Metaflex photonic devices can provide multiple channel reading for chem/biosensing applications.

In summary, SRR based Metaflex operating in the visible−IR optical frequency regime has been experimentally realized by EBL. We demonstrated the least line width of fabrication on plastic substrate ∼30 nm, which exhibited the lowest electric resonance near 542 nm and a magnetic response near 756 nm. Flexible metamaterials, particularly the magnetic resonance of them, exhibit high sensitivity response to strain, local dielectric environment, and surface chemical change in the visible−IR region, with a sensitivity as high as 436 nm/RIU, which we attribute to the electric and magnetic field coupling in SRRs. As two model chemical/biological sensing applications, we demonstrate that our flexible metamaterials exhibited a sensitivity of ∼4.5 nm/nM for nonspecific BSA protein binding, and an extraordinary 65 nm peak shift due to a monolayer of 2-naphthalenethiol molecule covalent binding. With recent progress in large scale imprinting lithography,[56] our work suggests that Metaflex operating in the visible−IR region exhibits numerous potential applications in large scale, low-cost, transparent, and portable photonic devices for strain and chemical/biological sensing.

AUTHOR INFORMATION

Corresponding Author
*E-mail: Qihua@ntu.edu.sg.

ACKNOWLEDGMENT

Q.X. acknowledges strong support from Singapore National Research Foundation through a NRF fellowship grant (NRF-RF2009-06), start-up grant support (M58113004), and New Iniative Fund (M58110100) from Nanyang Technological University (NTU). We thank Teijin DuPont Films Company for free PEN substrates and Dr. Daniel Aili for providing BSA sample.

REFERENCES

(1) Gelinck, G. H.; Huitema, H. E. A.; van Veenendaal, E.; Cantatore, E.; Schrijnemakers, L.; van der Putten, J. B. P. H.; Geuns, T. C. T.; Beenhakkers, M.; Giesbers, J. B.; Huisman, B.-H.; Meijer, E. J.; Benito, E. M.; Touwslager, F. J.; Marsman, A. W.; van Rens, B. J. E.; de Leeuw, D. M. *Nat. Mater.* **2004**, *3*, 106–110.

(2) Rogers, J. A.; Bao, Z.; Baldwin, K.; Dodabalapur, A.; Crone, B.; Raju, V. R.; Kuck, V.; Katz, H.; Amundson, K.; Ewing, J.; Drzaic, P. *Proc. Natl. Acad. Sci. U.S.A.* **2001**, *98*, 4835–4840.

(3) Fan, Z.; Razavi, H.; Do, J.-w.; Moriwaki, A.; Ergen, O.; Chueh, Y.-L.; Leu, P. W.; Ho, J. C.; Takahashi, T.; Reichertz, L. A.; Neale, S.; Yu, K.; Wu, M.; Ager, J. W.; Javey, A. *Nat. Mater.* **2009**, *8*, 648–653.

(4) McAlpine, M. C.; Friedman, R. S.; Jin, S.; Lin, K.-h.; Wang, W. U.; Lieber, C. M. *Nano Lett.* **2003**, *3*, 1531–1535.

(5) Someya, T.; Kato, Y.; Sekitani, T.; Iba, S.; Noguchi, Y.; Murase, Y.; Kawaguchi, H.; Sakurai, T. *Proc. Natl. Acad. Sci. U.S.A.* **2005**, *102*, 12321–12325.

(6) Takei, K.; Takahashi, T.; Ho, J. C.; Ko, H.; Gillies, A. G.; Leu, P. W.; Fearing, R. S.; Javey, A. *Nat. Mater.* **2010**, *9*, 821–826.

(7) McAlpine, M. C.; Ahmad, H.; Wang, D.; Heath, J. R. *Nat. Mater.* **2007**, *6*, 379–384.

(8) Leonhardt, U.; Tyc, T. *Science* **2009**, *323*, 110–112.

(9) Pendry, J. B.; Schurig, D.; Smith, D. R. *Science* **2006**, *312*, 1780–1782.

(10) Pryce, I. M.; Aydin, K.; Kelaita, Y. A.; Briggs, R. M.; Atwater, H. A. *Nano Lett.* **2010**, *10*, 41–48.

(11) Smith, D. R.; Pendry, J. B.; Wiltshire, M. C. K. *Science* **2004**, *305*, 788–792.

(12) Linden, S.; Enkrich, C.; Wegener, M.; Zhou, J.; Koschny, T.; Soukoulis, C. M. *Science* **2004**, *306*, 1351.

(13) Yen, T. J.; Padilla, W. J.; Fang, N.; Vier, D. C.; Smith, D. R.; Pendry, J. B.; Basov, D. N.; Zhang, X. *Science* **2004**, *303*, 1494.

(14) Enkrich, C.; Wegener, M.; Linden, S.; Burger, S.; Zschiedrich, L.; Schmidt, F.; Zhou, J. F.; Koschny, T.; Soukoulis, C. M. *Phys. Rev. Lett.* **2005**, *95*, 203901.
(15) Shalaev, V. M.; Cai, W.; Chettiar, U. K.; Yuan, H. K.; Sarychev, A. K.; Drachev, V. P.; Kildishev, A. V. *Opt. Lett.* **2005**, *30*, 3356.
(16) Zheludev, N. I. *Science* **2010**, *328*, 582–583.
(17) Melik, R.; Unal, E.; Perkgoz, N. K.; Puttlitz, C.; Demir, H. V. *Appl. Phys. Lett.* **2009**, *95*, 181105.
(18) Tao, H.; Strikwerda, A. C.; Fan, K.; Bingham, C. M.; Padilla, W. J.; Zhang, X.; Averitt, R. D. *J. Phys. D: Appl. Phys.* **2008**, *41*, 232004.
(19) Falco, A. D.; Ploschner, M.; Krauss, T. F. *New J. Phys.* **2010**, *12*, 113006.
(20) Pendry, J.; Holden, A.; Robbins, D.; Stewart, W. *IEEE Trans. Microwave Theory Tech.* **1999**, *47*, 2075–2084.
(21) Xu, X.; Quan, B.; Gu, C.; Wang, L. *J. Opt. Soc. Am. B* **2006**, *23*, 1174–1180.
(22) Shelby, R.; Smith, D.; Schultz, S. *Science* **2001**, *292*, 77.
(23) Liu, N.; Guo, H.; Fu, L.; Kaiser, S.; Schweizer, H.; Giessen, H. *Nat. Mater.* **2007**, *7*, 31–37.
(24) Oskooi, A. F.; Roundy, D.; Ibanescu, M.; Bermel, P.; Joannopoulos, J. D.; Johnson, S. G. *Comput. Phys. Commun.* **2010**, *181*, 687–702.
(25) Blaber, M. G.; Arnold, M. D.; Ford, M. J. *J. Phys. Chem. C* **2009**, *113*, 3041–3045.
(26) Rockstuhl, C.; Lederer, F.; Etrich, C.; Zentgraf, T.; Kuhl, J.; Giessen, H. *Opt. Express* **2006**, *14*, 8827–8836.
(27) Liu, N.; Giessen, H. *Angew. Chem., Int. Ed.* **2010**, *49*, 9838–9852.
(28) Driscoll, T.; Andreev, G. O.; Basov, D. N.; Palit, S.; Cho, S. Y.; Jokerst, N. M.; Smith, D. R. *Appl. Phys. Lett.* **2007**, *91*, 062511.
(29) Jain, P. K.; Huang, W.; El-Sayed, M. A. *Nano Lett.* **2007**, *7*, 2080–2088.
(30) Sonnichsen, C.; Reinhard, B. M.; Liphardt, J.; Alivisatos, A. P. *Nat. Biotechnol.* **2005**, *23*, 741–745.
(31) Melik, R.; Unal, E.; Perkgoz, N. K.; Puttlitz, C.; Demir, H. V. *Opt. Express* **2010**, *18*, 5000–5007.
(32) Liedberg, B.; Nylander, C.; Lundström, I. *Sens. Actuators* **1983**, *4*, 299–304.
(33) Lal, S.; Link, S.; Halas, N. J. *Nat. Photonics* **2007**, *1*, 641–648.
(34) Chen, H.; Ming, T.; Zhao, L.; Wang, F.; Sun, L.-D.; Wang, J.; Yan, C.-H. *Nano Today* **2010**, *5*, 494–505.
(35) Anker, J. N.; Hall, W. P.; Lyandres, O.; Shah, N. C.; Zhao, J.; Van Duyne, R. P. *Nat. Mater.* **2008**, *7*, 442–453.
(36) Kabashin, A. V.; Evans, P.; Pastkovsky, S.; Hendren, W.; Wurtz, G. A.; Atkinson, R.; Pollard, R.; Podolskiy, V. A.; Zayats, A. V. *Nat. Mater.* **2009**, 867–871.
(37) Gu, Y.; Li, Q.; Xiao, J.; Wu, K.; Wang, G. P. *J. Appl. Phys.* **2011**, *109*, 023104–6.
(38) Yanik, A. A.; Huang, M.; Kamohara, O.; Artar, A.; Geisbert, T. W.; Connor, J. H.; Altug, H. *Nano Lett.* **2010**, *10*, 4962–4969.
(39) Liu, N.; Weiss, T.; Mesch, M.; Langguth, L.; Eigenthaler, U.; Hirscher, M.; So nnichsen, C.; Giessen, H. *Nano Lett.* **2009**, *10*, 1103–1107.
(40) Liu, N.; Mesch, M.; Weiss, T.; Hentschel, M.; Giessen, H. *Nano Lett.* **2010**, *10*, 2342–2348.
(41) Micro.Chem. www.microchem.com/products/pdf/PMMA_Data_Sheet.pdf
(42) Marqués, R.; Medina, F.; Rafii-El-Idrissi, R. *Phys. Rev. B* **2002**, *65*, 144440.
(43) Liedberg, B.; Nylander, C.; Lundström, I. *Biosens. Bioelectron.* **1995**, *10*, 1–9.
(44) Shelton, D. J.; Peters, D. W.; Sinclair, M. B.; Brener, I.; Warne, L. K.; Basilio, L. I.; Coffey, K. R.; Boreman, G. D. *Opt. Express* **2010**, *18*, 1085–1090.
(45) Zheng, G.; Patolsky, F.; Cui, Y.; Wang, W. U.; Lieber, C. M. *Nat. Biotechnol.* **2005**, *23*, 1294–1301.
(46) Zheng, G.; Gao, X. P. A.; Lieber, C. M. *Nano Lett.* **2010**, *10*, 3179–3183.
(47) Jeppesen, C.; Xiao, S.; Mortensen, N. A.; Kristensen, A. *Opt. Express* **2010**, *18*, 25075–25080.
(48) Fedotov, V. A.; Rose, M.; Prosvirnin, S. L.; Papasimakis, N.; Zheludev, N. I. *Phys. Rev. Lett.* **2007**, *99*, 147401.
(49) Ulman, A. *Chem. Rev.* **1996**, *96*, 1533–1554.
(50) Kolega, R. R.; Schlenoff, J. B. *Langmuir* **1998**, *14*, 5469–5478.
(51) Alvarez-Puebla, R. A.; Dos Santos, D. S., Jr; Aroca, R. F. *Analyst* **2004**, *129*, 1251–1256.
(52) Zayak, A. T.; Hu, Y. S.; Choo, H.; Bokor, J.; Cabrini, S.; Schuck, P. J.; Neaton, J. B. *Phys. Rev. Lett.* **2011**, *106*, 083003.
(53) Leung, K. L.; Easteal, A. J. *J. Appl. Polym. Sci.* **2010**, *116*, 1442–1449.
(54) Theiss, J.; Pavaskar, P.; Echternach, P. M.; Muller, R. E.; Cronin, S. B. *Nano Lett.* **2010**, *10*, 2749–2754.
(55) Papasimakis, N.; Luo, Z.; Shen, Z. X.; De Angelis, F.; Di Fabrizio, E.; Nikolaenko, A. E.; Zheludev, N. I. *Opt. Express* **2010**, *18*, 8353–8359.
(56) Ahn, S. H.; Guo, L. J. *ACS Nano* **2009**, *3*, 2304–2310.